Eur. Phys. J. C 53, 689–699 (2008)
DOI 10.1140/epjc/s10052-007-0519-9

THE EUROPEAN PHYSICAL JOURNAL C

Special Article – Scientific Note

ATLAS sensitivity to Wtb anomalous couplings in top quark decays

J.A. Aguilar-Saavedra[1], J. Carvalho[2], N. Castro[2,a], A. Onofre[2], F. Veloso[2]

[1] Departamento de Física Teórica y del Cosmos and CAFPE, Universidad de Granada, 18071 Granada, Spain
[2] LIP, Dep. Física, Universidade de Coimbra, 3004-516 Coimbra, Portugal

Received: 22 June 2007 / Revised version: 14 December 2007 /
Published online: 10 January 2008 –

Abstract. We study the sensitivity of the ATLAS experiment to Wtb anomalous couplings in top pair production with semileptonic decay, $pp \to t\bar{t} \to W^+bW^-\bar{b}$ with one of the W bosons decaying leptonically and the other hadronically. Several observables are examined, including the W helicity fractions and new quantities recently introduced, such as the ratios of helicity fractions and some angular asymmetries defined in the W rest frame. The dependence on anomalous couplings of all these observables has been previously obtained. In this work we show that some of the new observables also have smaller systematic uncertainties than the helicity fractions, with a similar or stronger dependence on anomalous couplings. Consequently, their measurement can significantly improve the limits on anomalous couplings. Moreover, the most sensitive measurements can be combined. In this case, the precision achieved in the determination of Wtb anomalous couplings can be of a few percent in the semileptonic channel alone.

1 Introduction

The three generation structure of the standard model (SM) was completed with the discovery of the top quark at tevatron [1, 2]. Its properties have already been directly investigated at colliders [3–8] and, in particular, its mass has been determined to a high accuracy [9], better than for any other quark. However, the determination of other fundamental properties, like spin and couplings, requires larger top samples, which will be available at LHC. In its first low luminosity phase (10 fb^{-1}/year) LHC will produce several millions of top quarks per year and experiment, mainly in pairs through gluon fusion $gg \to t\bar{t}$ and quark–antiquark annihilation $q\bar{q} \to t\bar{t}$, with a total cross section of 833 pb for a top mass $m_t = 175$ GeV [10, 11]. Single top production [12–14] will also occur, dominated by the process $bq \to tq'$, with an expected cross section of 306 pb [10]. Both processes will test the SM predictions for the fundamental properties of the top quark, and in particular they will allow us to measure its couplings [12, 15–17]. This fact is specially important since, from a theoretical point of view, sizeable deviations from the SM predictions for top couplings are possible in several SM extensions, as for example in supersymmetry [21] and models of dynamical symmetry breaking [22]. Indeed, within the SM the Wtb coupling is purely left-handed at the tree level, and its size is given by the Cabibbo–Kobayashi–Maskawa (CKM) matrix element $V_{tb} \simeq 1$. But in SM extensions departures from the SM expectation for V_{tb} are possible [18–20], as well as new radiative contributions to the Wtb vertex. These deviations might be observed in top pair and single top production at LHC.

Top pair production takes place mainly through QCD interactions, thus independently of the electroweak Wtb coupling. Additionally, it is likely that the top quark almost exclusively decays in the channel $t \to W^+b$. Therefore, the cross section for $gg, q\bar{q} \to t\bar{t} \to W^+bW^-\bar{b}$ is insensitive to the size of the Wtb vertex, as well as to its chiral and tensorial structure. Still, the angular distributions of top decay products give information about the Wtb vertex structure (up to a global multiplicative constant), and thus they can be used to probe anomalous top couplings.[1] In the rest frame of a decaying top quark, the energies of the W boson and b quark are fixed by the two-body kinematics. Therefore, non-standard Wtb interactions can only influence the following groups of observables:

1. The total width $\Gamma(t \to Wb)$, which is very difficult to measure at LHC.[2]

[a] e-mail: nuno.castro@lipc.fis.uc.pt

[1] The global normalisation of the Wtb vertex can be determined in single top production, whose cross section is proportional to $|V_{tb}|^2$ plus terms involving anomalous couplings. Hence, the complete determination of the Wtb coupling requires the combination of measurements in single top and top pair production.

[2] The SM expectation, $\Gamma(t \to Wb) \sim 1.6$ GeV at the tree level, is one order of magnitude smaller than the width of the top invariant mass distribution reconstructed in the detector, which is about 12 GeV (see for example [23]). Thus, deviations from the SM prediction for the top quark width are not likely to be observable.

2. The helicity fractions of the W boson, which also determine the angular distributions of its decay products in the W rest frame and their energy distributions in the top rest frame.
3. The angular distribution of the W in the top rest frame, with respect to the top spin direction.

The second class of observables, those related to W helicity fractions, may be defined (and in principle measured) for the decay of a top quark independently of the production mechanism, centre of mass energy, etc. In particular, these observables can be measured in single top as well as in top pair production. Previous literature [24] has already studied the sensitivity of the ATLAS experiment [25] for the measurement of helicity fractions in top pair production and subsequent semileptonic or dileptonic decay. Here we extend that analysis by including additional observables defined in [26]: the ratios of helicity fractions (denoted as "helicity ratios") and some new angular symmetries defined in the W rest frame. The dependence on anomalous couplings of the observables in the second class has been obtained in [26], including quadratic terms and keeping the b quark mass nonzero. In particular, it has been found that some of the new observables in [26] have a stronger parametric dependence on anomalous couplings than helicity fractions. In this work we study in detail the ATLAS sensitivity for their measurement in the semileptonic channel, paying a special attention to systematic uncertainties, both the theoretical ones and those related to the measurement in a real detector. We will eventually find that some of the new observables have smaller systematic uncertainties, and that their measurement can significantly improve the precision in the determination of anomalous couplings.

This paper is organised as follows. In Sect. 2 we briefly set our notation and define the observables studied. A more extensive discussion of the theoretical aspects such as the relations among observables, their analytical expressions and plots of their dependence on anomalous couplings can be found in [26]. In Sect. 3 the generation of the $t\bar{t}$ signal and backgrounds is outlined, together with the selection criteria used to analyse them. In Sect. 4 we present our results for the expected experimental measurement of the observables considered, and in Sect. 5 we discuss their implications for the experimental determination of Wtb anomalous couplings. Section 6 is devoted to our conclusions.

2 The effective Wtb vertex and angular distributions in W rest frame

The most general Wtb vertex containing terms up to dimension five can be written as

$$\mathcal{L} = -\frac{g}{\sqrt{2}}\bar{b}\gamma^\mu (V_\mathrm{L}P_\mathrm{L} + V_\mathrm{R}P_\mathrm{R})tW_\mu^- - \frac{g}{\sqrt{2}}\bar{b}\frac{\mathrm{i}\sigma^{\mu\nu}q_\nu}{M_W}(g_\mathrm{L}P_\mathrm{L} + g_\mathrm{R}P_\mathrm{R})tW_\mu^- + \mathrm{h.c.}\,, \qquad (1)$$

with $q = p_t - p_b$ the W boson momentum. The new anomalous couplings V_R, g_L and g_R [15,26] can be related to f_1^R, f_2^L and f_2^R in [24] (and references therein) as $f_1^\mathrm{R} = V_\mathrm{R}$, $f_2^\mathrm{L} = -g_\mathrm{L}$ and $f_2^\mathrm{R} = -g_\mathrm{R}$. If we assume CP is conserved these couplings can be taken to be real. Within the SM, $V_\mathrm{L} \equiv V_{tb} \simeq 1$ and the other couplings vanish at the tree level, while small nonzero values are generated at one loop level in the SM [27] and its extensions (see for example [21,22]).

The measurement of angular distributions and asymmetries in top decays can only determine ratios of couplings. (Besides, a moderate deviation from $V_\mathrm{L} \simeq 1$ is not visible in top pair production and decay, as long as the top quark mainly decays to W^+b and all other channels are rare.) Then, the value of V_L sets the global scale for the measurement of V_R, g_L and g_R in top decays. In this work we will normalise V_L to unity, and the limits on anomalous couplings presented correspond to $V_\mathrm{L} = 1$. For any other value, the corresponding limits on anomalous couplings can be obtained by multiplying by the new V_L.

It must be noted that, apart from the direct measurement at LHC, low-energy measurements already set indirect limits on non-standard Wtb couplings. The size of a V_R term is constrained by the measured rate of $\mathrm{Br}(b \to s\gamma) = (3.3 \pm 0.4) \times 10^{-4}$ [28]. A right-handed coupling $|V_\mathrm{R}| \gtrsim 0.04$ would in principle give a too large contribution to this decay [29–31] which, however, might be (partially) cancelled with other new physics contributions. Hence, the bound $|V_\mathrm{R}| \leq 0.04$ is model dependent and does not substitute a direct measurement of this coupling. For g_L the limits from $b \to s\gamma$ are of the same order, while for g_R they are much looser [32]. Besides, if one allows all anomalous couplings to be nonzero, direct and indirect limits turn out to be complementary, because they constrain different combinations of anomalous couplings.

As we have already pointed out, the polarisation of the W bosons produced in the top decay is sensitive to non-standard Wtb couplings [33]. W bosons can be produced with positive, negative or zero helicity, with corresponding partial widths Γ_R, Γ_L, Γ_0 which depend on V_L, V_R, g_L and g_R. (General expressions for Γ_R, Γ_L, Γ_0 in terms of these couplings can be found in [26].) Their absolute measurement is rather difficult, so it is convenient to consider instead the helicity fractions $F_i \equiv \Gamma_i/\Gamma$, with $\Gamma = \Gamma_\mathrm{R} + \Gamma_\mathrm{L} + \Gamma_0$ the total width for $t \to Wb$. Within the SM, $F_0 = 0.703$, $F_\mathrm{L} = 0.297$, $F_\mathrm{R} = 3.6 \times 10^{-4}$ at the tree level, for $m_t = 175\,\mathrm{GeV}$, $M_W = 80.39\,\mathrm{GeV}$, $m_b = 4.8\,\mathrm{GeV}$. We note that F_R vanishes in the $m_b = 0$ limit because the b quarks produced in top decays have left-handed chirality, and for vanishing m_b the helicity and chirality states coincide. These helicity fractions can be measured in leptonic decays $W \to \ell\nu$. Let us denote by θ_ℓ^* the angle between the charged lepton three-momentum in the W rest frame and the W momentum in the t rest frame. The normalised angular distribution of the charged lepton can be written as

$$\frac{1}{\Gamma}\frac{\mathrm{d}\Gamma}{\mathrm{d}\cos\theta_\ell^*} = \frac{3}{8}(1+\cos\theta_\ell^*)^2 F_\mathrm{R} + \frac{3}{8}(1-\cos\theta_\ell^*)^2 F_\mathrm{L} + \frac{3}{4}\sin^2\theta_\ell^* F_0\,, \qquad (2)$$

with the three terms corresponding to the three helicity states and vanishing interference [34]. A fit to the $\cos\theta_\ell^*$ distribution allows to extract from experiment the values of F_i, which are not independent but satisfy $F_\mathrm{R}+F_\mathrm{L}+F_0=1$. From these measurements one can constrain the anomalous couplings in (1). Alternatively, from this distribution one can measure the helicity ratios [26]

$$\rho_\mathrm{R,L} \equiv \frac{\Gamma_\mathrm{R,L}}{\Gamma_0} = \frac{F_\mathrm{R,L}}{F_0}\,, \tag{3}$$

which are independent quantities and take the tree-level values $\rho_\mathrm{R}=5.1\times10^{-4}$, $\rho_\mathrm{L}=0.423$ in the SM. As for the helicity fractions, the measurement of helicity ratios sets bounds on V_R, g_L and g_R.

A third and simpler method to extract information about the Wtb vertex is through angular asymmetries involving the angle θ_ℓ^*. For any fixed z in the interval $[-1,1]$, one can define an asymmetry

$$A_z = \frac{N(\cos\theta_\ell^*>z)-N(\cos\theta_\ell^*<z)}{N(\cos\theta_\ell^*>z)+N(\cos\theta_\ell^*<z)}\,. \tag{4}$$

The most obvious choice is $z=0$, giving the forward–backward (FB) asymmetry A_FB [15,35].[3] The FB asymmetry is related to the W helicity fractions by

$$A_\mathrm{FB} = \frac{3}{4}[F_\mathrm{R}-F_\mathrm{L}]\,. \tag{5}$$

Other convenient choices are $z=\mp(2^{2/3}-1)$. Defining $\beta=2^{1/3}-1$, we have

$$\begin{aligned} z=-(2^{2/3}-1) &\to A_z=A_+=3\beta[F_0+(1+\beta)F_\mathrm{R}]\,,\\ z=(2^{2/3}-1) &\to A_z=A_-=-3\beta[F_0+(1+\beta)F_\mathrm{L}]\,. \end{aligned} \tag{6}$$

Thus, A_+ (A_-) only depend on F_0 and F_R (F_L). The SM tree-level values of these asymmetries are $A_\mathrm{FB}=-0.2225$, $A_+=0.5482$, $A_-=-0.8397$. They are very sensitive to anomalous Wtb interactions, and their measurement allows us to probe this vertex without the need of a fit to the $\cos\theta_\ell^*$ distribution. We also point out that with a measurement of two of these asymmetries the helicity fractions and ratios can be reconstructed. For instance, using (6) and requiring $F_\mathrm{R}+F_\mathrm{L}+F_0=1$, it is found that

$$\begin{aligned} F_\mathrm{R} &= \frac{1}{1-\beta}+\frac{A_--\beta A_+}{3\beta(1-\beta^2)}\,,\\ F_\mathrm{L} &= \frac{1}{1-\beta}-\frac{A_+-\beta A_-}{3\beta(1-\beta^2)}\,,\\ F_0 &= -\frac{1+\beta}{1-\beta}+\frac{A_+-A_-}{3\beta(1-\beta)}\,. \end{aligned} \tag{7}$$

[3] Notice the difference in sign with respect to the definitions in [15,35], where the angle $\theta_{\ell b}=\pi-\theta_\ell^*$ between the charged lepton and b quark is used.

3 Simulation of signals and backgrounds and event selection

The $t\bar{t}\to W^+bW^-\bar{b}$ events in which one of the W bosons decays hadronically and the other one in the leptonic channel $W\to\ell\nu_\ell$ (with $\ell=e^\pm,\mu^\pm$), are considered as signal events. (From now on, the W boson decaying hadronically and its parent top quark will be named as "hadronic", and the W decaying leptonically and its parent top quark will be called "leptonic".) Any other decay channel of the $t\bar{t}$ pair constitutes a background to this signal. Top pair production, as well as the background from single top production, is generated with TopReX 4.10 [36] with default settings. Further backgrounds without top quarks in the final state, i.e. $b\bar{b}$, $W+$jets, Z/γ^*+jets, WW, ZZ and ZW production processes, are generated using PYTHIA 6.206 [37]. In all cases we use CTEQ5L parton distribution functions (PDFs) [38]. Events are hadronised using PYTHIA, taking also into account initial state radiation (ISR), final state radiation (FSR) and pile-up.

The generated background and signal events are passed through the ATLAS fast simulation packages ATLFAST 2.53 [39] and ATLFASTB [39]. These packages simulate the energy deposition in the calorimeter cells of all the stable particles in each event. The calorimeter cells are clustered within a cone of $\Delta R=\sqrt{(\Delta\phi)^2+(\Delta\eta)^2}=0.4$, with ϕ the azimuthal angle and η the pseudorapidity. Cells with transverse energy $E_\mathrm{T}>1.5\,\mathrm{GeV}$ are used as cluster seeds and the cone algorithm is applied in decreasing order of E_T. Only clusters with $E_\mathrm{T}>5\,\mathrm{GeV}$ are considered. The polar angle and the momentum of photons are smeared according to Gaussian parameterisations. For electrons, their momenta are smeared according to a Gaussian parameterisations. The momentum of each muon is smeared according to a resolution which depends on the transverse momentum p_T, as well as on $|\eta|$ and ϕ. The photon (electron) energy resolution is $\delta E/E<2.9\%$ (3.3%), for $E>20\,\mathrm{GeV}$. The transverse momentum resolution of muons with $p_\mathrm{T}<100\,\mathrm{GeV}$ is $\delta p_\mathrm{T}/p_\mathrm{T}\lesssim 2\%$. Photons, electrons and muons are selected only if they have $|\eta|<2.5$ and $p_\mathrm{T}>5\,\mathrm{GeV}$ ($p_\mathrm{T}>6\,\mathrm{GeV}$ for muons). They are classified as isolated if the transverse energy of the cluster associated to the particle, inside a cone of $\Delta R=0.2$, does not exceed the particle energy by 10 GeV, and the ΔR from other energy clusters must be above 0.4. The clusters of energy depositions not associated to isolated photons, electrons or muons are used for the jet reconstruction. Their momenta are smeared according to a Gaussian distribution which depends on $|\eta|$. Jets are selected if they have $E_\mathrm{T}>10\,\mathrm{GeV}$. For $E>20\,\mathrm{GeV}$, the jet energy resolution is better than 12% (for pseudorapidities $|\eta|<3$) and better than 24% (for $|\eta|>3$). The missing transverse momentum is estimated by summing the transverse momentum of the isolated photons, electrons, muons and jets. The non-isolated muons and the clusters of energy deposition which are not associated to isolated photons, electrons, muons or jets, are also taken into account. In the ATLAS detector, it will be possible to identify b jets with $|\eta|<2.5$ by using b tagging tools. The algorithm was simulated by setting a b-tagging efficiency to 60%, with contamination factors set to 14.9%

and 1.1% for c jets and light jets, respectively (the latter from light quark, gluon and tau leptons). In order to check the dependence of the analysis with the b-tagging efficiencies, different values, 50% and 70% (corresponding to the expected b-tag variation within the interesting signal transverse momentum range), were also considered for the systematic studies, with contamination factors of 9.2% (0.4%) and 23.3% (2.9%) for c-jets (light jets).

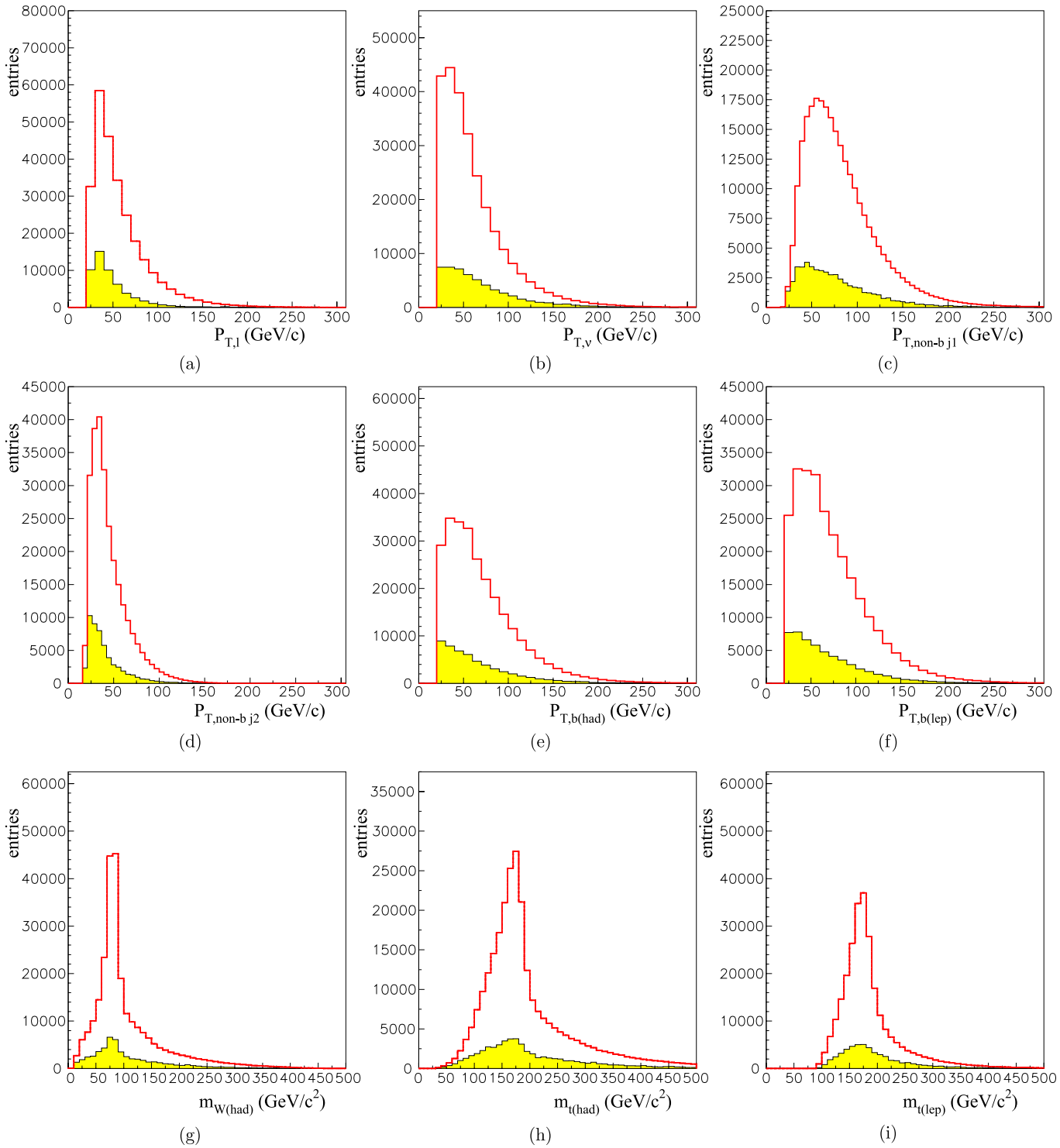

Fig. 1. Kinematical distributions at the pre-selection level for the transverse momentum of the charged lepton (**a**), the neutrino (**b**), the p_{T} of the two non b jets used in the hadronic W reconstruction (**c**,**d**), the b jet from the hadronic (**e**) and leptonic (**f**) top quarks. Invariant mass distributions of the hadronic W boson (**g**), the hadronic top (**h**) and the leptonic top (**i**). The $t\bar{t}$ signal (*full line*) and the SM backgrounds (*shaded region*) are normalised to $L = 10\,\mathrm{fb}^{-1}$

Due to the hadronisation and FSR, the jets are reconstructed with less energies than those from the original quarks or gluons. The jet energies are calibrated by the ATLFASTB package, by applying a calibration factor, $K^{\rm jet} = p_{\rm T}^{\rm parton}/p_{\rm T}^{\rm jet}$, which is the ratio between the true parton energy and the reconstructed jet energy, obtained from reference samples [39]. The calibration factor depends on $p_{\rm T}$ and is different for b-tagged and light jets.

Signal events have a final state topology characterised by one isolated lepton (the isolation criterium requires the absence of additional tracks with $p_{\rm T} > 10\,{\rm GeV}$ inside a cone of $\Delta R = 0.4$ around the lepton direction), at least four jets (among which exactly two must be tagged as b jets) and large transverse missing energy. We apply a two-level probabilistic analysis, based on the construction of a discriminant variable which uses the full information of some kinematical properties of the event. In the first level (called the pre-selection), a cleaner sample is obtained accepting events with: (i) exactly one charged lepton with $p_{\rm T} > 25\,{\rm GeV}$, $|\eta| < 2.5$; (ii) at least 4 jets with $p_{\rm T} > 20\,{\rm GeV}$, $|\eta| < 2.5$, two of them tagged as b jets and at least two not b-tagged; (iii) missing transverse momentum above 20 GeV. The number of signal and background events (normalised to $L = 10\,{\rm fb}^{-1}$) and the signal efficiency after the pre-selection are shown in the first column of Table 1. Distributions of relevant variables are presented in Fig. 1.

The hadronic W reconstruction is done from the two non-b jets with highest transverse momentum. The invariant mass of these two jets is represented in Fig. 1 at the pre-selection. The mass of the hadronic top , also shown in Fig. 1, is reconstructed as the invariant mass of the hadronic W and the b jet (among the two with highest $p_{\rm T}$) closer to the W. The leptonic W momentum cannot be directly reconstructed due to the presence of an undetected neutrino in the final state. Nevertheless, the neutrino four-momentum can be estimated by assuming the transverse missing energy to be the transverse neutrino momentum. Its longitudinal component can then be determined, with a quadratic ambiguity, by constraining the leptonic W mass (calculated as the invariant mass of the neutrino and the charged lepton) to its known on-shell value $M_W \simeq 80.4\,{\rm GeV}$. In order to solve the twofold quadratic ambiguity in the longitudinal component it is required that the hadronic and the leptonic top quarks have the minimum mass difference. The reconstructed mass of the leptonic top is shown in Fig. 1 at the pre-selection.

Table 1. Number of signal $t\bar{t} \to \ell\nu b\bar{b}q\bar{q}'$ and background events, normalised to $L = 10\,{\rm fb}^{-1}$, after the pre-selection and final selection. The $b\bar{b}$ background is negligible after selection

Process	Pre-selection	Final selection
$t\bar{t} \to \ell\nu b\bar{b}q\bar{q}'$	262 111 (11%)	220 024 (9%)
$t\bar{t}$ (other)	36 745	27 060
Single t	12 410	7600
Z + jets	566	253
W + jets	3627	1307
WW, ZZ, ZW	109	51
Total SM bkg.	53 457	36 271

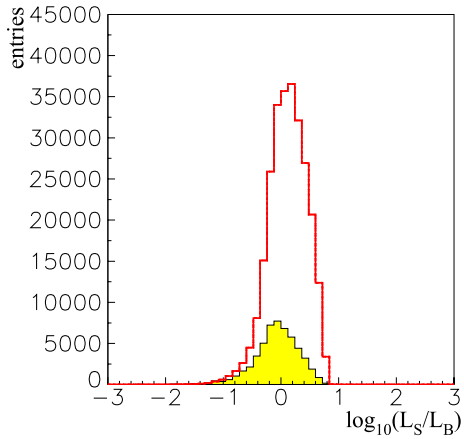

Fig. 2. Discriminant variable for the SM background (*shaded region*) and the $t\bar{t}$ signal (*full line*), normalised to $L = 10\,{\rm fb}^{-1}$

In the second level (the final selection), for each event we construct signal and background-like probabilities, $\mathcal{P}_i^{\rm sig.}$ and $\mathcal{P}_i^{\rm back.}$, respectively, using probability density functions (p.d.f.) built from relevant physical variables:

- The hadronic W mass.
- The hadronic and leptonic top masses.
- The transverse momentum of the b-jets associated to the hadronic and the leptonic top quarks.
- The transverse momentum of the jets used in the hadronic W reconstruction.

These seven variables are shown in Fig. 1c–i. Signal ($\mathcal{L}_S = \Pi_{i=1}^n \mathcal{P}_i^{\rm sig.}$) and background ($\mathcal{L}_B = \Pi_{i=1}^n \mathcal{P}_i^{\rm back.}$) likelihoods (with $n = 7$, the number of p.d.f.) are used to define a discriminant variable $L_{\rm R} = \log_{10} \mathcal{L}_S/\mathcal{L}_B$. This variable is shown in Fig. 2 for the signal and background. The final event selection is done by applying a cut $L_{\rm R} > -0.2$ on the discriminant variable, which corresponds to the highest $S/\sqrt{B}$ ratio. The number of background events (normalised to $L = 10\,{\rm fb}^{-1}$) and signal efficiency after the final selection are shown in the second column of Table 1.

Two more cut-based analyses, omitted here for brevity, have also been performed. The results obtained depend more on the top mass reconstruction method than on the type (cut-based or probabilistic) of analysis performed. A detailed comparison of the three of them can be found in [40], where it is shown that the probabilistic analysis presented here gives the best results, with smaller systematic uncertainties.

4 Experimental measurement of angular distributions and asymmetries

The experimentally observed $\cos\theta_\ell^*$ distribution, which includes the $t\bar{t}$ signal as well as the SM backgrounds, is af-

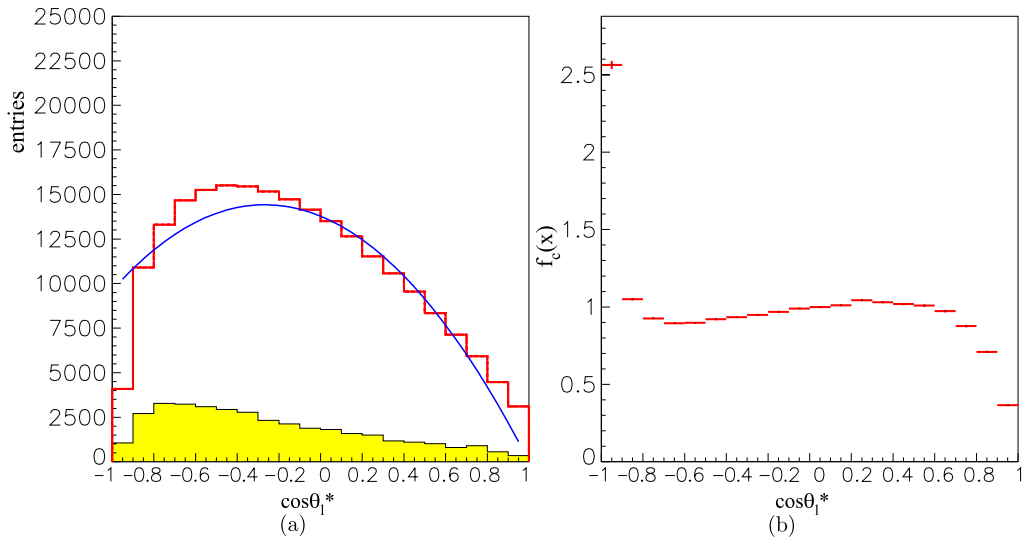

Fig. 3. Simulated $\cos\theta_\ell^*$ distribution (**a**) and its correction function (**b**). In the first plot the $t\bar{t}$ signal (*full line*) and the SM backgrounds (*shaded region*) are normalised to $L = 10\,\text{fb}^{-1}$

Table 2. Theoretical and reconstructed values of helicity fractions, helicity ratios and angular asymmetries, with their statistical errors for $L = 10\,\text{fb}^{-1}$

	F_0	F_L	F_R	ρ_L	ρ_R	A_FB	A_+	A_-
Th.	0.703	0.297	3.6×10^{-4}	0.423	5.1×10^{-4}	−0.2220	0.5493	−0.8402
Rec.	0.700	0.299	0.0006	0.4274	0.0004	−0.2231	0.5472	−0.8387
Δ stat.	0.003	0.003	0.0012	0.0080	0.0021	0.0035	0.0032	0.0018

fected by detector resolution, $t\bar{t}$ reconstruction and selection criteria. In order to recover the theoretical distribution, it is necessary to: (i) subtract the background; (ii) correct for the effects of the detector, reconstruction, etc. For this purpose, we use two different sets of signal and background event samples: one "experimental" set, which simulates a possible experimental result, and one "reference" set, which is used to parameterise the effects mentioned and correct the previous sample. The procedure is as follows. After subtracting reference background samples, the "experimental" distribution is multiplied by a correction function f_c in order to recover the theoretical one expected in the SM.[4] The correction function is calculated, for each bin of the $\cos\theta_\ell^*$ distribution, dividing the number of events at the generator level by the number of events after the event selection, using the reference sample. The "experimental" $\cos\theta_\ell^*$ distribution obtained after the simulation is shown in Fig. 3, together with the correction function obtained from the reference sample. The asymmetries are measured with a simple counting of the number of events below and above a specific value of $\cos\theta_\ell^*$ as in (6). The procedure to correct for detector and reconstruction effects is basically the same, but with the $\cos\theta_\ell^*$ distribution divided into two or three bins. This has the advantage that the asymmetry measurements are not biased by the extreme values of the angular distributions, where correction functions largely deviate from unity and special care is required (see Fig. 3). The helicity fractions and ratios obtained from a fit to the corrected distribution, as well as the angular asymmetries A_FB, $A_\pm$, are collected in Table 2, with their statistical uncertainties. For easy comparison, we also include the theoretical values obtained at the generator level.

Due to the excellent statistics achievable at LHC, which is apparent in Table 2, systematic errors play a crucial role in the measurement of angular distributions and asymmetries for a luminosity of $10\,\text{fb}^{-1}$ or larger. A thorough discussion of the different systematic uncertainties in the determination of the correction functions is therefore compulsory. We estimate the systematic errors in the observables studied (asymmetries, helicity fractions and ratios) by calculating them with various reference samples and observing the differences obtained. In some cases the estimates are conservative, and they are taken as a reference for better comparison with previous analyses [24]. We consider uncertainties originating from:

Monte Carlo generator: The correction functions obtained from a sample generated with TopReX are applied to a sample generated with ALPGEN [41]. The

[4] Correction functions are determined assuming that the charged lepton distribution corresponds to the SM one. In case that a deviation from SM predictions (corresponding to anomalous couplings) is found, the correction function must be modified accordingly, and the theoretical distribution recalculated in an iterative process. These issues have been analysed in detail in [24], where it is shown that this process quickly converges.

difference between the values obtained at the generator level and after the simulation is considered as systematic uncertainty.

Structure functions: The correction functions obtained from a reference sample generated with CTEQ5L PDFs are applied to samples generated with CTEQ6L and MRST 2001 PDFs in order to estimate the effects on the correction functions, and thus on the observables. The most significant deviations found are considered as the systematic error associated to the structure functions.

Top mass dependence: Samples corresponding to top masses of 170, 175 and 180 GeV are simulated, and the influence of m_t on the values obtained for the corrected observables (using correction functions for $m_t = 175$ GeV) is determined. The systematic error used here is obtained from a linear fit of the values found corresponding to a top mass uncertainty of 2 GeV.

ISR and FSR: Their effect is studied following [42]. An event sample is created in which ISR and FSR are switched off in the event simulation. We compare the results of the reference sample (with ISR and FSR) with those obtained adding to it a normalised fraction of the sample without ISR nor FSR (from 0% to 25%, in steps of 5%). The values obtained for the observables are fitted with a linear function and the systematic error is considered as the effect of the presence of 20% (a conservative estimate of our level of knowledge of ISR and FSR) of the sample without ISR, FSR.

b jet tag efficiency: The value of the b jet tag efficiency (and the corresponding c jet and light jet rejection factors) is varied from 50 to 70%, in steps of 5%, and the values obtained for the observables are fitted with a linear function The systematic error is considered as the effect on the observables of a variation of 5% in the b jet tagging efficiency, as compared with the standard value of 60%.

b jet energy scale: The value of the b jet energy scale is changed from -5 to $+5$%, and the values obtained for the observables are fitted with a linear function. The systematic error is considered as the effect of a variation of 3% in the b jet energy scale.

Light jet energy scale: The value of the energy scale of the light jets is changed from -3 to $+3$%, and the values obtained for the observables are fitted with a linear function. The systematic error is considered as the effect of a variation of 1% in the energy scale of the light jets.

Background: The background (as obtained from the reference sample) subtracted to the selected sample is varied from -25 to 25%, in steps of 5%, and the values obtained for the observables are fitted with a linear function. The systematic error is considered as the effect of a variation of 10% on the background level (which takes into account the uncertainties in the cross-sections).

Pile-up: The effect of pile-up events (2.3 events in average) is studied by comparing the values of the observables obtained with and without adding pile-up events.

b quark fragmentation: The parameter ϵ_b in the Peterson parameterisation for b quark fragmentation is changed from -0.006 to -0.0035, and the values obtained for the observables compared. The difference is considered as systematic error [42].

The systematic errors in each observable, resulting from these theoretical and simulation uncertainties, are collected in Table 3. It can be observed that $\rho_{\rm R}$ and A_- have very small total systematic errors. In the case of $\rho_{\rm R}$, the improvement over $F_{\rm R}$ is due to the cancellation of some of the systematic errors in the ratio, while the opposite happens in the case of $\rho_{\rm L}$, compared to $F_{\rm L}$.

The reduction of systematic errors compared to previous analyses deserves an explanation. In this analysis the W helicity fractions and ratios are obtained by fitting the angular distribution from -0.99 to $+0.99$, and it should be stressed that a dependence of the systematic error with the range of the fit has been observed. If the fit is performed between -0.89 and $+0.89$, the systematic errors on F_0, $F_{\rm L}$ and $F_{\rm R}$ are respectively 0.0206, 0.0188 and 0.0033 (in good agreement with the results of [24]). However, if the fit is performed in the range $[-0.89, +0.99]$ the results are respectively 0.0190, 0.0182 and 0.0017, still in good agreement with the values on Table 3. This implies that the correct reconstruction of the most extreme bins of the angular distribution is of utmost importance in order to control the error associated to the W polarisation measurements, if the fitting method is used. In the case of the asymmetries, for $A_\pm$ the smaller errors are due to the greater stabil-

Table 3. Sources of systematic errors in the determination of helicity fractions, helicity ratios and angular asymmetries

Source	F_0	$F_{\rm L}$	$F_{\rm R}$	$\rho_{\rm L}$	$\rho_{\rm R}$	$A_{\rm FB}$	A_+	A_-
MC generator	0.0002	0.0002	0.0004	0.0006	0.0000	0.0035	0.0015	0.0006
PDFs	0.0032	0.0022	0.0009	0.0046	0.0008	0.0021	0.0005	0.0014
Top mass	0.0065	0.0060	0.0006	0.0124	0.0007	0.0034	0.0039	0.0005
ISR + FSR	0.0116	0.0113	0.0003	0.0218	0.0001	0.0046	0.0049	0.0011
b tag eff.	0.0065	0.0062	0.0003	0.0126	0.0003	0.0039	0.0046	0.0004
E_b scale	0.0028	0.0030	0.0002	0.0061	0.0002	0.0021	0.0017	0.0005
E_j scale	0.0034	0.0037	0.0002	0.0074	0.0002	0.0038	0.0023	0.0014
Back.	0.0001	0.0000	0.0000	0.0001	0.0000	0.0001	0.0000	0.0001
Pile-up	0.0091	0.0086	0.0005	0.0175	0.0002	0.0080	0.0051	0.0006
b frag.	0.0049	0.0037	0.0012	0.0078	0.0011	0.0045	0.0000	0.0012
Total Δ sys.	0.0189	0.0178	0.0018	0.0356	0.0016	0.0130	0.0099	0.0028

Table 4. Summary of the results obtained from the simulation for the observables studied, including statistical and systematic uncertainties

Observable	Result		
F_0	0.700	± 0.003 (stat.)	± 0.019 (sys.)
F_L	0.299	± 0.003 (stat.)	± 0.018 (sys.)
F_R	0.0006	± 0.0012 (stat.)	± 0.0018 (sys.)
ρ_L	0.4274	± 0.0080 (stat.)	± 0.0356 (sys.)
ρ_R	0.0004	± 0.0021 (stat.)	± 0.0016 (sys.)
A_FB	-0.2231	± 0.0035 (stat.)	± 0.0130 (sys.)
A_+	0.5472	± 0.0032 (stat.)	± 0.0099 (sys.)
A_-	-0.8387	± 0.0018 (stat.)	± 0.0028 (sys.)

ity of these measurements, obtained by counting events, compared to observables obtained from a fit to the $\cos\theta_\ell^*$ distribution. We point out that the selection of z for the definition of $A_\pm$ in (6) has not been optimised in order to achieve smaller systematic errors. Instead, these asymmetries have been defined in a simple way which allows to reconstruct easily the helicity fractions, using (7). The results of our simulation, including statistical and systematic uncertainties, are summarised in Table 4.

5 Limits on anomalous couplings

With the results obtained in the previous section, summarised in Table 4, and the parametric dependence of the observables on V_R, g_L and g_R implemented in the computer program TopFit [26], constraints on the latter can be set. Naively, to obtain the 1σ limit on a coupling $x = V_\mathrm{R}, g_\mathrm{L}, g_\mathrm{R}$ derived from the measurement of some observable O, one would simply find the values of x for which O deviates 1σ from its central value.[5] Nevertheless, due to the quadratic dependence of the observables on V_R and g_L near the SM point $V_\mathrm{R} = g_\mathrm{L} = 0$, this procedure leads to overcoverage of the obtained confidence intervals [26], because their p.d.f. is not Gaussian even if the p.d.f. of the observable O is. In order to obtain the limits on an anomalous coupling x, given by the measurement of an observable O, we determine the p.d.f. of x numerically, using the acceptance-rejection method: we iteratively (i) generate a random value (with uniform probability) x_i within a suitable interval; (ii) evaluate the probability of $O(x_i)$, given by the p.d.f. of O; (iii) generate an independent random number r_i (with uniform probability); and (iv) accept the value x_i if the probability of $O(x_i)$ is larger than r_i. The resulting set of values $\{x_i\}$ is distributed according to the p.d.f. of x given by the measurement of O. The determination of a central interval with a given CL γ is done numerically, requiring: (a) that it contains a fraction γ of the total number of values $\{x_i\}$; (b) that is central, i.e. fractions $(1-\gamma)/2$ of the values generated are on each side of the interval.

For $x = g_\mathrm{R}$ this method gives results very similar to the intersection method in [24, 40], whereas for V_R and g_L the confidence intervals found are 20% and 30% smaller, respectively. The 1σ limits derived from the measurement of each observable are collected in Table 5, assuming only one nonzero coupling at a time. We notice the improvement in sensitivity brought by the new observables $\rho_\mathrm{R,L}$ and $A_\pm$: the best limits on V_R and g_L are obtained from the measurement of ρ_R, improving the limits from F_R by a factor of 1.13, and the best limits on g_R are provided by A_+, improving the limits from F_L by a factor of 1.34. This is due to the smaller (systematic plus statistical) uncertainties of these new observables and their stronger dependence on anomalous couplings.

These limits can be further improved by combining the measurements of the four observables $\rho_\mathrm{R,L}$ and $A_\pm$, including their correlations. We point out that the correlations among $A_\pm$, $\rho_\mathrm{R,L}$ do depend (as they must) on the method followed to extract these observables from experimental data. In our analysis $A_\pm$ are obtained by a simple event counting above and below a specific value of $z = \cos\theta_\ell^*$, while $\rho_\mathrm{R,L}$ are obtained from a fit to the $\cos\theta_\ell^*$ distribution, divided in 20 bins. The correlations among these observables are derived as follows. We use a set of hypothetical "experimental measurements", in which each element of the set is a binned $\cos\theta_\ell^*$ distribution, as it would be experimentally obtained after correcting for detector effects. For each "measurement", the number of events in each $\cos\theta_\ell^*$ bin is obtained randomly using a Gaussian distribution centered at the expected SM value. We then calculate the average on this set, denoted by $\langle\cdot\rangle$, of the ten independent products of observables $\langle A_+^2\rangle$, $\langle A_+ A_-\rangle$, $\langle A_+\rho_\mathrm{L}\rangle$, etc., where $A_\pm$, $\rho_\mathrm{R,L}$ are extracted from the $\cos\theta_\ell^*$ distribution as indicated above.[6] The resulting correlation matrix is shown in Table 6. The correlations among $A_\pm$ and $\rho_\mathrm{R,L}$ obtained are not affected by systematic uncertainties, as long as these do not significantly distort the shape of the $\cos\theta_\ell^*$ distribution with respect to the SM one.

When the four observables $A_\pm$ and $\rho_\mathrm{R,L}$ are combined the assumption that only one coupling is nonzero can be relaxed. However, if V_R and g_L are simultaneously allowed to be arbitrary, the limits on them are very loose and correlated, because for fine-tuned values of these couplings their effects on helicity fractions cancel to a large extent. In this way, values $O(0.4)$ of V_R and g_L are possible yielding minimal deviations on the observables studied. Therefore, in our combined limits, which are presented in Table 7, we require that either V_R or g_L vanishes. Limits for both V_R, g_L nonzero require additional observables beyond the ones di-

[5] This is the procedure originally followed in our previous work [40], as well as in [24]: For an observable O and a coupling x, intersecting the plot of $O(x)$ with the two horizontal lines $O = O_\mathrm{exp} \pm \Delta O$, which correspond to the 1σ variation of O, gives the pretended 1σ interval on x.

[6] Since the four observables $A_\pm$, $\rho_\mathrm{R,L}$ are obtained from the corrected $\cos\theta_\ell^*$ distribution, there is no need to know the full kinematics of the $t\bar{t}$ event in order to determine their statistical correlation. On the other hand, if we are interested in, for example, the correlation between one of these observables and a top-antitop spin asymmetry, the full $t\bar{t}$ kinematics is needed. In the latter case, systematic errors can possibly influence the determination of the correlations.

Table 5. Limits on anomalous couplings obtained by the measurement of the observables in the left column, with the constraint that only one non-standard coupling is allowed to be nonzero at a time. Dashes are shown where there is no significant sensitivity

	$V_{\rm R}$ $(g_{\rm L} = g_{\rm R} = 0)$	$g_{\rm L}$ $(V_{\rm R} = g_{\rm R} = 0)$	$g_{\rm R}$ $(V_{\rm R} = g_{\rm L} = 0)$
F_0	–	$[-0.133, 0.102]$	$[-0.0315, 0.0219]$
$F_{\rm L}$	$[-0.196, 0.186]$	$[-0.167, 0.136]$	$[-0.0293, 0.0212]$
$F_{\rm R}$	$[-0.0373, 0.1070]$	$[-0.0491, 0.0169]$	–
$\rho_{\rm L}$	$[-0.254, 0.206]$	–	$[-0.0275, 0.0227]$
$\rho_{\rm R}$	$[-0.0282, 0.0987]$	$[-0.0455, 0.0129]$	–
$A_{\rm FB}$	$[-0.118, 0.148]$	$[-0.0902, 0.0585]$	$[-0.0268, 0.0227]$
A_+	$[-0.140, 0.146]$	$[-0.112, 0.0819]$	$[-0.0213, 0.0164]$
A_-	$[-0.0664, 0.120]$	$[-0.0620, 0.0299]$	$[-0.0166, 0.0282]$

Table 6. Correlation matrix for $A_\pm$, $\rho_{\rm R,L}$

	A_+	A_-	$\rho_{\rm L}$	$\rho_{\rm R}$
A_+	1	0.1587	−0.8222	−0.1232
A_-	0.1587	1	−0.08583	0.5688
$\rho_{\rm L}$	−0.8222	−0.08583	1	0.3957
$\rho_{\rm R}$	−0.1232	0.5688	0.3957	1

rectly related to W helicity fractions, and will be presented elsewhere.

For completeness, and to compare with previous literature we also present the 2σ limits on non-standard couplings when only one of them is nonzero,

$$\begin{aligned} V_{\rm R}(2\sigma) \quad & [-0.0566, 0.128] \qquad (g_{\rm L} = g_{\rm R} = 0)\,, \\ g_{\rm L}(2\sigma) \quad & [-0.0579, 0.0258] \qquad (V_{\rm R} = g_{\rm R} = 0)\,, \\ g_{\rm R}(2\sigma) \quad & [-0.0260, 0.0312] \qquad (V_{\rm R} = g_{\rm L} = 0)\,. \end{aligned} \tag{8}$$

A significant improvement, by factors of 3.25, 3.1 and 1.4, respectively, is obtained with the present analysis with respect to the results presented in [24], which include the dilepton channel as well. This improvement is mainly due to:

(i) The better sensitivity of the observables used. In the case of $g_{\rm L}$ and $V_{\rm R}$ the improvement is moderate, with limits about 1.13 times smaller. For $g_{\rm R}$ the improvement is more significant, by a factor of 1.34.

(ii) The combination of $\rho_{\rm R,L}$ and $A_\pm$.

(iii) The different statistical analysis used. For $V_{\rm R}$ and $g_{\rm L}$, the Monte Carlo method used to obtain the true 68.3% CL intervals also reduces their size by 20%–30%, as explained above.

Finally, with the same procedure we obtain the 68.3% CL confidence regions on the anomalous couplings, presented in Fig. 4. The boundary of the regions has been chosen as a contour of constant χ^2. In case that the p.d.f. of $V_{\rm R}$ and $g_{\rm L}$ were Gaussian, the boundaries would be ellipses corresponding to $\chi^2 = 2.30$ (see for instance [43]). In our non-Gaussian case the χ^2 for which the confidence regions have 68.3% probability is determined numerically, and it is approximately 1.83 for the $(g_{\rm L}, g_{\rm R})$ plot and 1.85 for $(V_{\rm R}, g_{\rm R})$.

6 Conclusions

In this paper we have investigated the ATLAS sensitivity to non-standard Wtb couplings. We have considered several observables: the helicity fractions F_i, helicity ratios $\rho_{\rm R,L}$ and angular asymmetries $A_{\rm FB}$, $A_\pm$. Although these observables can be defined and measured for any top production process with decay $t \to Wb \to \ell\nu b$, we have concentrated on top pair production at LHC with semileptonic decay, with a large cross section and in which the reconstruction of the final state is relatively easy.

Due to the excellent statistics available at LHC, the precision reached is determined by systematic uncertain-

Table 7. Limits on anomalous couplings obtained from the combined measurement of $A_\pm$, $\rho_{\rm R,L}$. In each case, the couplings which are fixed to be zero are denoted by a cross

	$V_{\rm R}$	$g_{\rm L}$	$g_{\rm R}$
$A_\pm$, $\rho_{\rm R,L}$	$[-0.0195, 0.0906]$	×	×
$A_\pm$, $\rho_{\rm R,L}$	×	$[-0.0409, 0.00926]$	×
$A_\pm$, $\rho_{\rm R,L}$	×	×	$[-0.0112, 0.0174]$
$A_\pm$, $\rho_{\rm R,L}$	×	$[-0.0412, 0.00944]$	$[-0.0108, 0.0175]$
$A_\pm$, $\rho_{\rm R,L}$	$[-0.0199, 0.0903]$	×	$[-0.0126, 0.0164]$

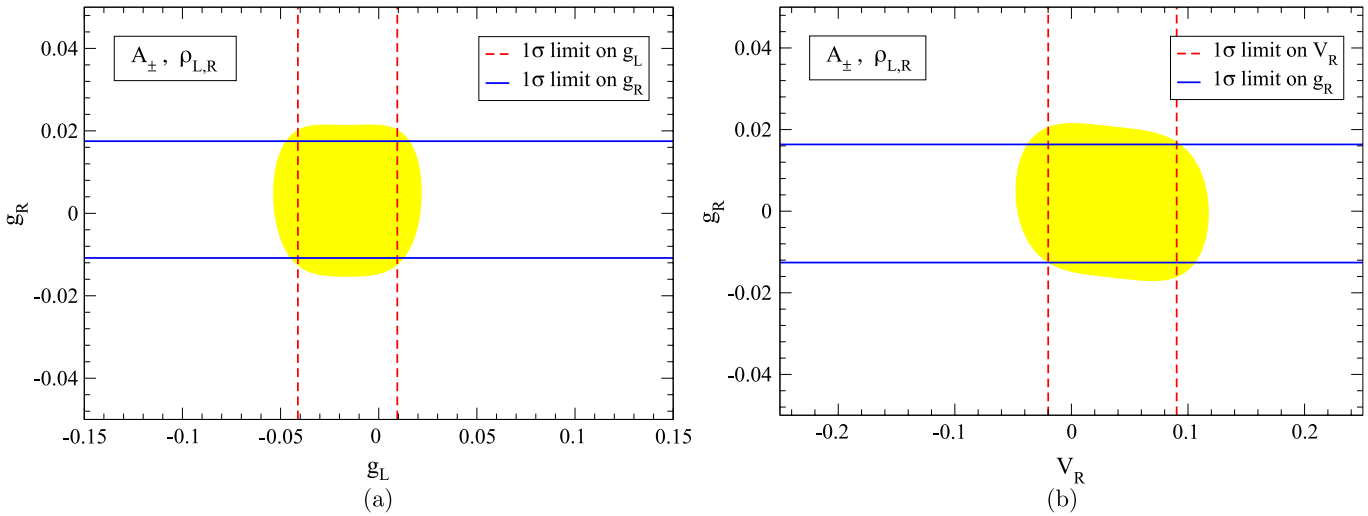

Fig. 4. 68.3% CL confidence regions on anomalous couplings: $g_{\rm L}$ and $g_{\rm R}$, for $V_{\rm R} = 0$ (**a**); $V_{\rm R}$ and $g_{\rm R}$, for $g_{\rm L} = 0$ (**b**). The 1σ combined limits in Table 7 are also displayed

ties. We have performed a very detailed study of the latter, both theoretical ones and from the experimental reconstruction. It has been found that, although the observables considered are theoretically equivalent (as noted in Sect. 2), the systematic uncertainties in the measurement of some of them, namely $\rho_{\rm R}$ and A_+, are smaller. Since these observables also depend more strongly on anomalous couplings, their measurement provides a more sensitive probe for anomalous Wtb couplings than helicity fractions. Moreover, when the four measurements of $\rho_{\rm R,L}$ and $A_\pm$ are combined, the sensitivity is further enhanced, reaching the 5.5%, 2.5% and 1.4% level for $V_{\rm R}$, $g_{\rm L}$ and $g_{\rm R}$ in (1), respectively. This is an important achievement for a hadronic machine. Combining this measurement in $t\bar{t}$ semileptonic decays with the dilepton decay channel $t\bar{t} \to \ell^+\nu b \ell'^-\nu\bar{b}$ and single top production will improve (to what extent is yet to be determined) these limits.

Although providing probably the strongest limits, the observables studied in this paper are not sufficient to fully constrain anomalous Wtb couplings in a model-independent way. For nonzero $V_{\rm R}$ and $g_{\rm L}$, even of order $O(0.4)$, there are fine-tuned combinations for which their effects on helicity fractions and related observables almost cancel. Setting simultaneous limits on them requires additional observables with a different functional dependence on the Wtb couplings. For example, in the dilepton channel two spin asymmetries $A_{\ell\ell'}$ and $\tilde{A}_{\ell\ell'}$ involving the two leptons are found to be sensitive to $V_{\rm R}$ but rather independent of $g_{\rm L}$ [26]. Reference [24] has shown that these asymmetries can be measured with a good precision, 7% and 5%, respectively, and their study seems very promising. Spin asymmetries involving b quarks like $A_{\ell b}$ and $\tilde{A}_{\ell b}$ exhibit a stronger dependence on anomalous couplings and when the appropriate detailed simulations are in place they will be studied. In addition single top production, involving Wtb interactions in the production and the decay of the top quark will be studied, since it can provide complementary information about non-standard couplings through the cross sections for the different final states tj, $\bar{t}j$, $t\bar{b}$ and $\bar{t}b$, and spin asymmetries.

Acknowledgements. This work has been performed within the ATLAS Collaboration, and we thank collaboration members for helpful discussions. We have made use of the physics analysis framework and tools which are the result of collaboration-wide efforts. The work of J.A.A.-S. has been supported by a MEC Ramon y Cajal contract and project FPA2006-05294, by Junta de Andalucía projects FQM 101 and FQM 437 and by the European Community's Marie-Curie Research Training Network under contract MRTN-CT-2006-035505 "Tools and Precision Calculations for Physics Discoveries at Colliders". The work of J.C., N.C. (grant SFRH/BD/13936/2003), A.O. and F.V. (grant SFRH/BD/18762/2004) has been supported by Fundação para a Ciência e a Tecnologia.

References

1. CDF Collaboration, F. Abe et al., Phys. Rev. Lett. **73**, 225 (1994) [hep-ex/9405005]
2. CDF Collaboration, F. Abe et al., Phys. Rev. D **50**, 2966 (1994)
3. D0 Collaboration, V.M. Abazov et al., Phys. Rev. D **75**, 031 102 (2007) [hep-ex/0609045]
4. CDF Collaboration, A. Abulencia et al., Phys. Rev. Lett. **98**, 072 001 (2007) [hep-ex/0608062]
5. CDF Collaboration, F. Abe et al., Phys. Rev. Lett. **80**, 2525 (1998)
6. D0 Collaboration, B. Abbott et al., Phys. Rev. Lett. **85**, 256 (2000) [hep-ex/0002058]
7. CDF Collaboration, A. Abulencia et al., Phys. Rev. Lett. **97**, 082 004 (2006) [hep-ex/0606017]
8. D0 Collaboration, V.M. Abazov et al., Phys. Rev. D **76**, 052 006 (2007) [0706.0458 [hep-ex]]
9. The Tevatron Electroweak Working Group, hep-ex/0703034, see also http://tevewwg.fnal.gov
10. M. Beneke et al., hep-ph/0003033

11. N. Kidonakis, R. Vogt, Phys. Rev. D **68**, 114014 (2003) [hep-ph/0308222]
12. T. Stelzer, Z. Sullivan, S. Willenbrock, Phys. Rev. D **58**, 094021 (1998) [hep-ph/9807340]
13. A.S. Belyaev, E.E. Boos, L.V. Dudko, Phys. Rev. D **59**, 075001 (1999) [hep-ph/9806332]
14. T. Tait, C.P. Yuan, Phys. Rev. D **63**, 014018 (2001) [hep-ph/0007298]
15. F. del Aguila, J.A. Aguilar-Saavedra, Phys. Rev. D **67**, 014009 (2003) [hep-ph/0208171]
16. D. Espriu, J. Manzano, Phys. Rev. D **66**, 114009 (2002) [hep-ph/0209030]
17. C.R. Chen, F. Larios, C.P. Yuan, Phys. Lett. B **631**, 126 (2005) [hep-ph/0503040]
18. J.A. Aguilar-Saavedra, Phys. Rev. D **67**, 035003 (2003) [hep-ph/0210112]
19. J.A. Aguilar-Saavedra, Phys. Rev. D **69**, 099901 (2004) [Erratum]
20. F. del Aguila, J. Santiago, JHEP **0203**, 010 (2002) [hep-ph/0111047]
21. J.J. Cao, R.J. Oakes, F. Wang, J.M. Yang, Phys. Rev. D **68**, 054019 (2003) [hep-ph/0306278]
22. X.L. Wang, Q.L. Zhang, Q.P. Qiao, Phys. Rev. D **71**, 014035 (2005) [hep-ph/0501145]
23. F. Hubaut, E. Monnier, P. Pralavorio, B. Resende, C. Zhu, ATLAS note ATL-PHYS-PUB-2006-017
24. F. Hubaut, E. Monnier, P. Pralavorio, K. Smolek, V. Simak, Eur. Phys. J. C **44**, 13 (2005) [hep-ex/0508061]
25. ATLAS Collaboration, ATLAS detector and physics performance technical design report, CERN-LHCC-99-15
26. J.A. Aguilar-Saavedra, J. Carvalho, N. Castro, A. Onofre, F. Veloso, Eur. Phys. J. C **50**, 519 (2007) [hep-ph/0605190]
27. H.S. Do, S. Groote, J.G. Korner, M.C. Mauser, Phys. Rev. D **67**, 091501 (2003) [hep-ph/0209185]
28. Particle Data Group, S. Eidelman et al., Phys. Lett. B **592**, 1 (2004)
29. F. Larios, M.A. Perez, C.P. Yuan, Phys. Lett. B **457**, 334 (1999) [hep-ph/9903394]
30. G. Burdman, M.C. Gonzalez-Garcia, S.F. Novaes, Phys. Rev. D **61**, 114016 (2000) [hep-ph/9906329]
31. K. Whisnant, J.M. Yang, B.L. Young, X. Zhang, Phys. Rev. D **56**, 467 (1997) [hep-ph/9702305]
32. M. Misiak, private communication, to appear in the WG1 report ("Collider aspects of flavour physics at high Q") of the workshop "Flavour in the era of the LHC", CERN 2005–2007
33. G.L. Kane, G.A. Ladinsky, C.P. Yuan, Phys. Rev. D **45**, 124 (1992)
34. R.H. Dalitz, G.R. Goldstein, Phys. Rev. D **45**, 1531 (1992)
35. B. Lampe, Nucl. Phys. B **454**, 506 (1995)
36. S.R. Slabospitsky, L. Sonnenschein, Comput. Phys. Commun. **148**, 87 (2002) [hep-ph/0201292]
37. T. Sjöstrand, P. Eden, C. Friberg, L. Lonnblad, G. Miu, S. Mrenna, E. Norrbin, Comput. Phys. Commun. **135**, 238 (2001) [hep-ph/0010017]
38. CTEQ Collaboration, H.L. Lai et al., Eur. Phys. J. C **12**, 375 (2000) [hep-ph/9903282]
39. E. Richter-Was, D. Froidevaux, L. Poggioli, ATLAS note ATL-PHYS-98-131
40. J.A. Aguilar-Saavedra, J. Carvalho, N. Castro, A. Onofre, F. Veloso, ATLAS note ATL-PHYS-PUB-2006-018
41. M.L. Mangano, M. Moretti, F. Piccinini, R. Pittau, A.D. Polosa, JHEP **0307**, 001 (2003) [hep-ph/0206293], see also http://mlm.home.cern.ch/m/mlm/www/alpgen/
42. I. Borjanovic et al., Eur. Phys. J. C **39**, 63 (2005) [hep-ex/0403021]
43. G. Cowan, Statistical Data Analysis (Oxford University Press, Clarendon, 1998)